EFFECT OF THERMO-MECHANICAL PROCESSING ON STRUCTURE AND PROPERTIES OF DUAL-PHASE MATRIX ADI WITH DIFFERENT SI-CONTENTS

M. Soliman and H. Palkowski
Institute of Metallurgy, Clausthal University of Technology, 38678 Clausthal-Zellerfeld, Germany

A. Nofal
Central Metallurgical Research and Development Institute (CMRDI), Helwan, Cairo 11421, Egypt

Abstract

The improvement in the combination between strength and ductility of austempered ductile iron with dual matrix structure was investigated in two ductile irons having different silicon contents, namely 2.6 wt% and 4.0 wt%. The structure was produced in a thermo-mechanical simulator, equipped with a dilatometry system. The effect of silicon content on the transformation kinetics and mechanical properties was studied. For both ductile irons, the influence of introducing ferrite into the matrix on the structure development and mechanical properties was investigated and compared to those of completely ausferritic matrix. Increasing the Si-content widened the intercritical region and shifted it to higher temperature range. The former effect renders the intercritical annealing process more controllable. The introduction of the ferrite phase accelerated the ausferrite transformation kinetics and improved both the ductility and the formability index (ductility × ultimate strength), while both yield and ultimate strength declined.

Keywords: *ADI, thermo-mechanical processing, dual-phase matrix, proeutectoid ferrite, ausferrite formation*

Introduction

The dual-phase matrix (DPM) ADI is a novel grade of ADI with optimal combination of strength/ductility properties that was developed with a matrix structure of a soft phase, which is the ferrite and a hard phase which is either martensite (DMS-M) [1,2] or ausferrite (acicular ferrite and high carbon austenite; DMS-ADI).[3–9] The DMS-ADI is produced by intercritical annealing (partial austenitization) in the intercritical region, where $\alpha + \gamma$ + graphite coexists and then austempering at 250–400 °C, thus small ferrite grains dispersed within the ausferrite matrix are formed (Figure 1).[4,5]

The DPM-ADI or as it is referred to sometimes in the literature as the intercritically austempered ductile iron (IADI) has recently drawn considerable interest due to its exciting properties, namely:

- The tensile and proof stresses of ductile irons with DMS are much higher than pearlitic and ferritic grades and ductility is slightly low.[2,9]
- Such combination of properties allows IADI to absorb more energy during deformation than either pearlitic or ferritic ductile irons, resulting in improved flaw tolerance and excellent fatigue properties combined with good machinability.[3,8]

It should be noted that, contrary to the conventional ADI, where the austempering time and temperature have the major effect on mechanical properties, intercritical austenitizing time and temperature of IADI significantly effect the mechanical properties since these determine the ratio of γ/α as well as the amount of carbon and other alloying elements into solid solution in γ. Moreover, the hardenability of austenite in IADI is not as high as the

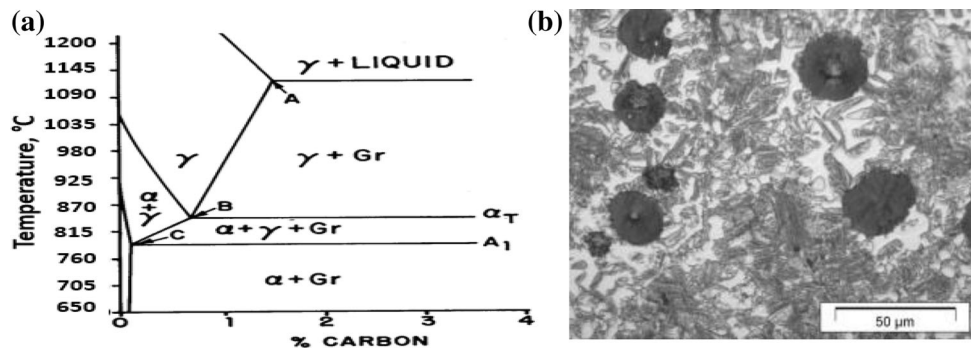*Figure 1. (a) A section of the Fe–C–2% Si equilibrium phase diagram, showing the intercritical region (α + γ + Gr) and (b) the microstructure of IADI where small ferrite grains are dispersed within the ausferrite matrix coexist together with ausferrite and graphite spheroids. The structure of (b) evolved by formation of austenite within the ferrite during heating at the intercritical temperature before quenching to transform the intercritical austenite to Af + RA.*

austenite in ADI due to lower C-content of austenite at lower austenitization temperatures.[10]

On the other hand, the hot deformation of ductile iron attracts attention, because it refines the austenite structures, closes up the internal shrinkage cavities and gas porosity, and reduces the segregations of alloying elements. Additionally, it increases the dimensional accuracy and surface finish of the products which would finally reduce the manufacturing cost. Forged ductile iron products have been promoted as replacements for some types of steel forgings.[11]

In the current work, controlling the microstructure and mechanical properties of ductile iron by combining both thermo-mechanical processing and controlling the proeutectoid ferrite volume fractions is introduced. In the current proposed process, the dissolution of carbide and refining of the matrix structure take place during the austenitization and the deformation processes, respectively, whereas the DMS is formed during the subsequent controlled thermal cycle. For the proposed process, the following points were investigated:

1- Studying the effect of silicon content on the kinetics of ferrite and ausferrite formation in the thermo-mechanically processed ductile iron.
2- Selecting thermal parameters depending on the results of this study.
3- Investigating the effects of both silicon content and introducing ferrite to the matrix on the compression properties.

Experimental Procedure

Material

Two ductile irons with two different Si-contents were investigated. The chemical compositions of the alloys are given in Table 1. About 1% Al is added to accelerate the ausferrite formation kinetics.[10] Melting was performed in an induction furnace. The Mg treatment to obtain nodular graphite was performed using Vortex method using 1.4 kg of 9.5 wt% MgFeSi master alloy for about 100 kg of molten melt. The Mg treatment was followed by post-inoculation with 0.5 kg of 75 wt% FeSi. The melt was cast in sand molds in form of Y-blocks with a size of 15 mm × 190 mm × 230 mm. The blocks were machined to a thickness of 10 mm to remove the cast surface structure.

Thermo-Mechanical Processing

For thermo-mechanical processing and dilatometric study, a Baehr Dil 805D thermo-mechanical simulator was used. A detailed description of the device is described elsewhere.[12] The thermo-mechanical simulation was performed on cylindrical samples of 5 mm diameter and 10 mm length. Sheathed type S "Pt/Pt-10% Rh" thermocouples with a nominal diameter of 0.2 mm were individually spot welded to the specimens' surface in central position. The deformation is performed using two quartz

Table 1. Compositions of the Ductile Irons (wt%)

DI	C	Si	Mn	Al	Mg	S	P
A1	3.57	2.59	0.33	0.96	0.046	0.011	0.025
A2	3.50	4.01	0.31	0.93	0.050	0.018	0.025

stamps. The dimensional variations of the specimens during the thermal-deformation cycle are transmitted via a moving quartz pushrod to a LVDT sensor. The thermal cycles were performed under vacuum of 0.005 Pa by inductive heating using a high frequency (HF) generator. Helium was used for cooling (Figure 2). The specimens were subjected to the thermo-mechanical schedule, namely "Schedule I" and "Schedule II" which are designated in Figure 3.

In both schedules, the specimens were heated up to 960 °C with a heating rate of 10 Ks^{-1} and subjected to two deformation steps of $\varphi_1 = 0.1$ and $\varphi_2 = 0.2$ at 960 °C and 940 °C, respectively, as shown in Figure 3; where φ_1 and φ_2 are the true compression strains. The main objective of these deformation steps is to refine the structure through work hardening, recovery and recrystallization effects in austenite. The very slow deformation rate of 0.5 s^{-1} was adopted to minimize the susceptibility of the specimen to cracking by decreasing the strain hardening effect during deformation. After the last deformation step, the material is either quenched to an austempering temperature (T_A) of 375 °C to form ausferrite (Af) + blocky retained austenite (RA) matrix or isothermally held at temperatures within the intercritical region (T_i), so as to form a certain amount of ferrite (F) before quenching to TA to finally obtain a matrix of (F + Af + RA). Subsequent to austempering the materials were quenched to room temperature (RT). Both of the quenching to RT and to T_A was performed with a cooling rate of 50 Ks^{-1}.

Characterization of the Microstructure and Mechanical Properties

To investigate microstructural constituents, the specimens were prepared by mechanical grinding followed by polishing up to a 0.2 μm-grade SiO_2 solution. The microstructures were examined with a light microscope after etching with 2% nital.
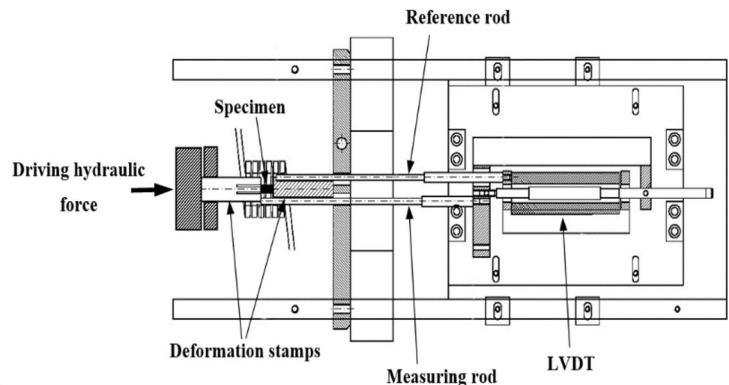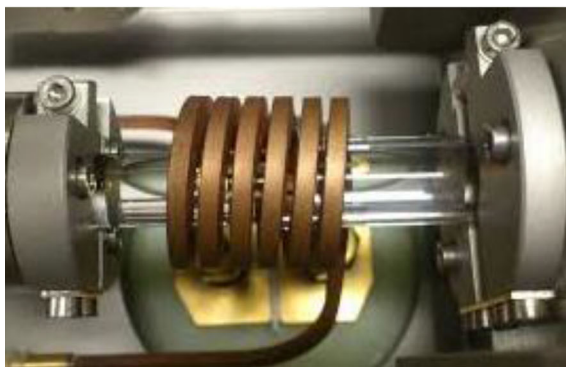
The mechanical properties for the alloys were determined in terms of the compression properties. Quasi static-compression tests were conducted in a computerized universal testing machine (UTS) at a crosshead speed of 1 mm/min on samples resulting from the simulation process. For each condition, at least four samples were tested.

Results and Discussions

As-cast Microstructure

Figure 4 shows the as-cast (AC) microstructures of the two DIs. The microstructure characteristics of the AC DIs are listed in Table 2. Both AC DIs showed ferritic pearlitic matrices. Increasing the Si results in reducing the pearlite in the matrix. The ferrite grain size is insignificantly affected by increasing the silicon. The average ferrite grain size of the as-cast structure recorded about 34 μm. The nodularity and the nodule size decreased significantly with increasing the Si, whereas the nodule count increased.

Evolution of the Structure

Ferrite Formation

The intercritical region, of both alloys, was characterized by applying both dilatometric and metallographic investigations. The detailed methodology for characterization of the intercritical region and selecting the temperatures corresponding to prescribed ferrite contents is described elsewhere.[12,13] This is achieved by slow heating in the intercritical region with a rate of 0.05 Ks^{-1} to trace the equilibrium points. Table 3 lists the critical temperatures of both alloys together with the intercritical annealing temperature (Ti) corresponding to a ferrite content of approximately 15% in the matrix, which is selected for intercritical annealing in "Schedule II". Increasing the Si-content widens the intercritical region and shifted it to a higher temperature range (Table 3), thus rendering the intercritical annealing process more controllable.

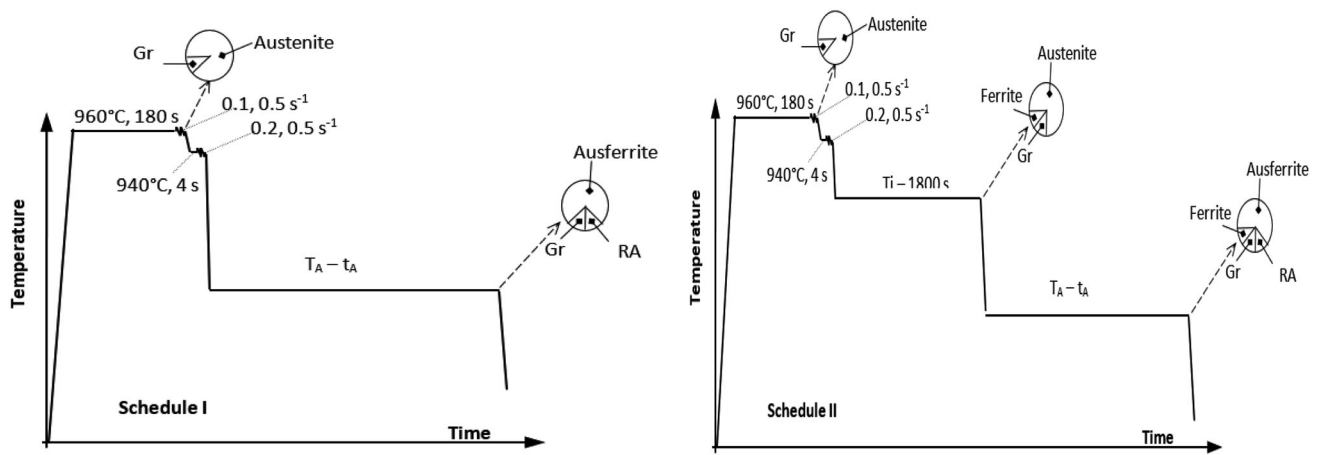**Figure 2. Experimental setup for Baehr Dil 805D thermo-mechanical simulator.**

Figure 3. Thermo-mechanical schedules applied on the two ductile irons; Gr: graphite, RA: retained austenite and Ti: intercritical annealing temperature.
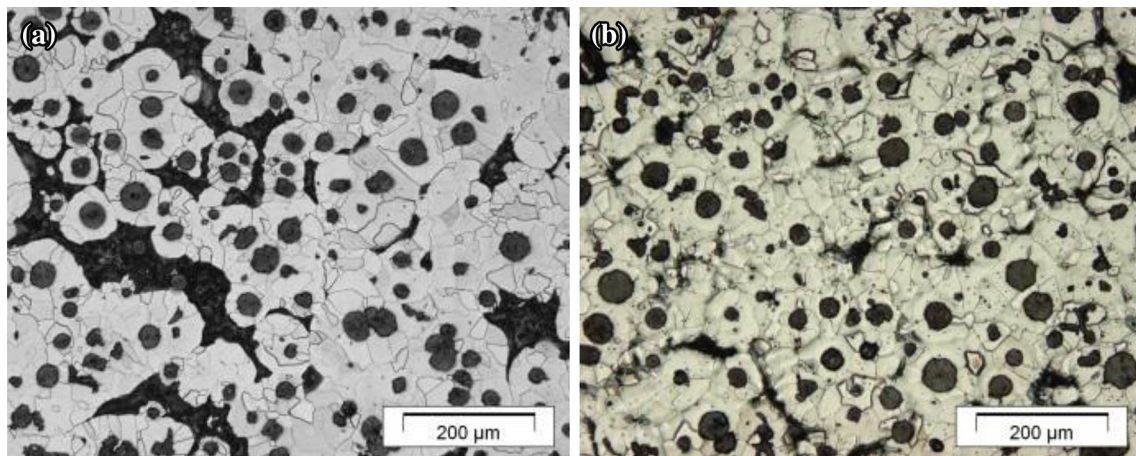

Figure 4. As-cast microstructure of ductile irons (a) A1 and (b) A2.

Table 2. Microstructure Characteristics of the as-Cast Structure

DI	Pearlite (%)	Nodule count (1/mm²)	Nodule size (μm)	Nodularity (%)
A1	19	325	20.5	67
A2	8	391	15.8	61

Table 3. Measured Critical Temperatures (Ae1 and Ae3) Together with the Estimated Intercritical Temperature (Ti) Corresponding to 15% Ferrite in the Matrix

DI	A_{e1} (°C)	Ti (°C)	A_{e3} (°C)
A1	771	815	850
A2	803	875	911

The evolution of ferrite was detected from the change in length of the specimens. The length change of both alloys during holding time at the selected Ti was monitored using the LVDT-system in Dil 805D. Figure 5 shows the kinetics of ferrite formation in terms of relative change in length. The transformation starts more quickly, due to an enhanced nucleation rate. The transformation then proceeds toward the interior of the austenite grains at a slower rate. Increasing the silicon content speeds up the ferrite formation kinetics as observed in Figure 5.

Ausferrite Formation

To obtain the ausferrite structure, specimens were quenched to 375 °C either after the last deformation step (Schedule I), or after intercritical annealing at Ti (Schedule II). For both cases, the ausferrite formation in terms of length change is given in Figure 6. This figure shows that the bainite reaction reaches a transformation stasis after different times depending on the alloy-composition and the applied schedule. The reason for this stasis of the reaction,
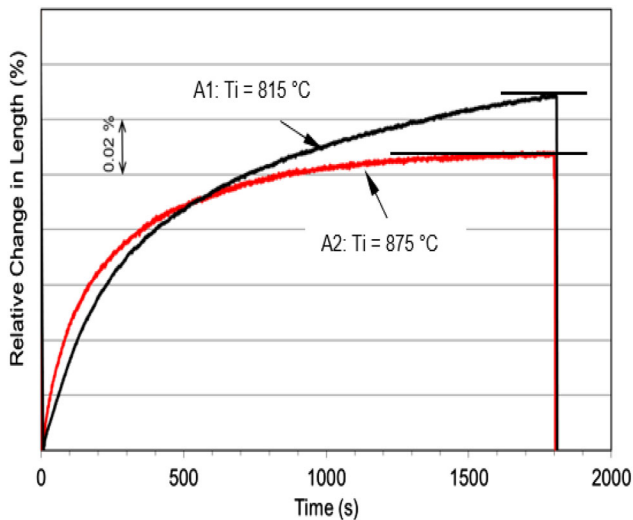
Figure 5. Ferrite formation in terms of length change during isothermal holding at the prescribed intercritical annealing temperatures, Ti (refer to Schedule II of Figure 3).

which limits the amount of bainitic ferrite that can be obtained at any temperature, is explained by the incomplete reaction theory. The reaction is said to be incomplete since transformation stops before the phases achieve their equilibrium compositions.[14] It is noted from Figure 6 that the kinetics of ausferrite formation is accelerated for the materials with proeutectoid ferrite phase (Schedule II). This observation is recorded for both alloys. This acceleration can be correlated to:

1- The increased number of sites for the nucleation of ausferrite at the ferrite/austenite interface.
2- The smaller amount of austenite to be transformed to ausferrite.
3- The lower C content of the intercritically annealed austenite as previously shown by Soliman et al.[10]
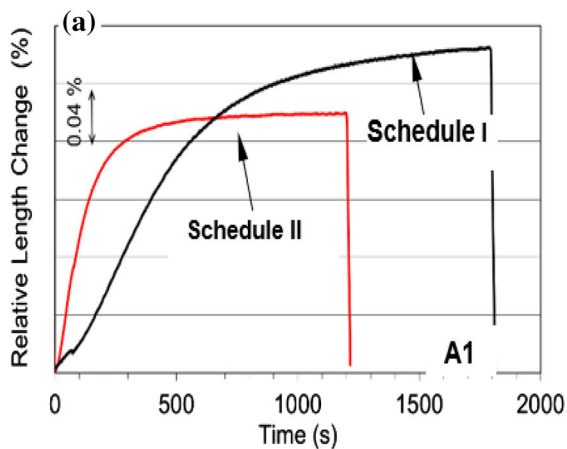
In the case of Schedule II the specimens are quenched to RT after 20 min. Prolonged holding would subject the ductile iron to the second stage of the austempering reaction in which ε-carbides precipitate from high carbon austenite. This would result in material embrittlement.[15]

The dilatation curves of Figure 6 indicate deforming the austenite before austempering results in decreasing the incubation period before the transformation to an insignificant value. Furthermore, introducing ferrite to the microstructure before austempering (Schedule II) results in an additional marked reduction in the incubation period.[10] Both factors (deformation and ferrite formation) provide sites for the nucleation of ausferrite during austempering, thus suppressing the incubation period of transformation.

The decrease in dilatation with increasing the Si-content observed in Figure 6b when comparing to Figure 6a does not necessarily imply a decrease in the quantity of the formed ausferrite. According to the mathematical model developed by Takahashi and Bhadeshia,[16] the increase in the lattice parameter due to increasing the alloying elements results in decreasing the total dilatation corresponding to the same quantity of the formed bainitic ferrite.

The structure obtained after austempering is shown in Figure 7. The elongated shape of the graphite nodules is due to subjecting the ductile iron to the two deformation steps with a total reduction $\varphi = 0.3$. The matrix of the specimens subjected to Schedule I consists of Af and RA. This indicates that the cooling rate of 50 Ks^{-1} was sufficient to suppress any transformation process before the austempering, i.e., avoiding the nose of the ferrite–pearlite. An additional ferrite phase appears in the matrix of the specimens subjected to Schedule II as shown in Figure 7e–h. The ferrite volume fraction in both specimens, as measured from the dilatometric and metallographic investigations, has an approximate value of 15%. In all cases, the ferrite is preferentially formed in the vicinity of the
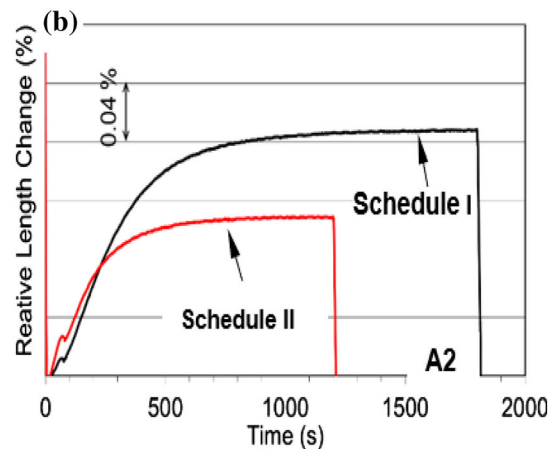

Figure 6. Ausferrite formation in terms of length change during isothermal holding at 375 °C of the prescribed schedule for (a) ductile iron A1 and (b) ductile iron A2.
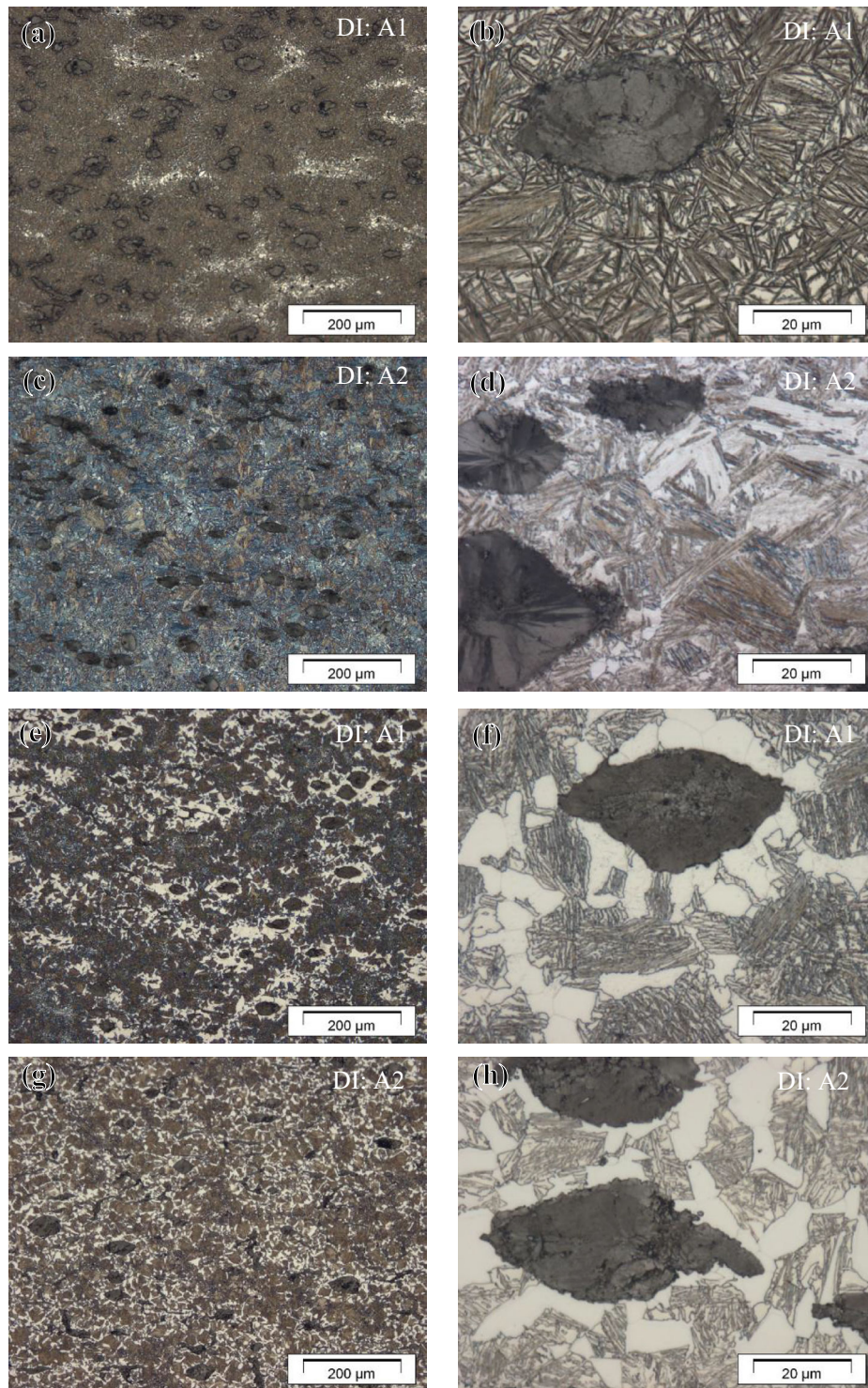
International Journal of Metalcasting/Volume 14, Issue 3, 2020

857

Figure 7. Microstructures of specimens: (a) to (d) subjected to Schedule I, and (e) to (h) subjected to Schedule II.

nodules. This preferential localization of ferrite around the nodule is associated with carbon diffusion from austenite to the graphite nodules *during cooling* and holding (refer to Schedule II of Figure 3). These regions are locations of lower carbon content compared to the interior of the austenite matrix due to the shorter diffusion distance of carbon atoms, thus the ferrite-nucleation at these regions is

motivated. Comparing these structures with that evolved, firstly by formation of austenite within the ferrite *during heating* at the intercritical temperature and then quenching to transform that austenite to Af + RA (like that structure shown in Figure 1b), it can be observed that the latter structure is more homogenously distributed.

Compression Properties

The mechanical properties for the alloys are determined by compression tests. Figure 8 shows representative true stress–true strain curves obtained by compression tests. The axial compression test has been used for investigating the ductile fracture limits of the material. This has been done by taking advantage of the barrel formation and controlled stress and strain conditions at the equator of the barreled surface when compression is carried out with friction. These stress and strain conditions lead to tensile stress around the circumference and reduce compressive stress at the bulge equator. Eventually, the surface is cracked due to the tensile stress in the circumferential direction at the bulge surface.[17] Table 4 shows that the introduction of the ferrite phase in the microstructure results in increased ductility at the expense of the strength. Furthermore, the solid solution strengthening effect of the increased silicon in alloy A2 manifests itself in terms of increase in yield strength (Rp); however the ultimate compression strength (Rm) and the fracture strain (FS) decline.

The formability index (F.I.) which is the product of the ultimate strength and the total elongation is calculated for both of the alloys.[12] The F.I. of the ausferritic ductile iron recorded values of 510 MPa and 464 MPa for A1 and A2, respectively. Introduction of the ferrite in the microstructure results in significant increase in the F.I. of alloy A1 to 587 MPa and its marginal increase in alloy A2 to 474 MPa.

Conclusions

This work highlights transformation kinetics, microstructure evolution and compression properties of two thermomechanically processed ductile irons having 2.6 wt% and 4
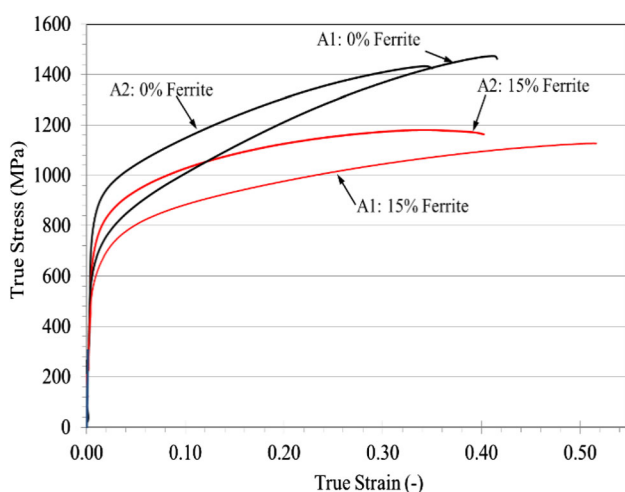
Table 4. Ultimate Compression Strength (Rm), Yield Strength (Rp), Fracture Strain (FS) and Formability Index (F.I.) of the Studied Ductile Irons

DI	Ferrite content (%)	Rm (MPa)	Rp (MPa)	FS (−)	FI (MPa)
A1	0	1418 ± 77	663 ± 45	0.36 ± 0.08	510
	15	1174 ± 69	622 ± 49	0.50 ± 0.14	587
A2	0	1405 ± 39	844 ± 44	0.33 ± 0.09	464
	15	1155 ± 43	751 ± 14	0.41 ± 0.09	474

wt% Si. Two types of matrices were produced in these ductile irons, namely ausferritic and ferritic–ausferritic matrices. In both alloys the introduction of the ferrite accelerates the ausferrite transformation kinetics and improves both, the compression ductility and formability index. However, the yield and ultimate strength decline. On the other hand, increasing the Si-content has a significant effect on speeding up the transformation kinetics of the ductile iron as revealed by the acceleration of ferrite formation observed at the intercritical temperature and ausferrite formation at the austempering temperature. The alloy with higher Si-content shows an improved yield strength but lower ultimate strength and ductility.

Figure 8. True stress–true strain curves obtained by compression test of specimens having the prescribed ferrite content.

REFERENCES

1. Y. Sahin, M. Erdogan, M. Cerah, Effect of martensite volume fraction and tempering time on abrasive wear of ferritic ductile iron with dual matrix. Wear **265**, 196–202 (2008)

2. K. Kocatepe, M. Cerah, M. Erdogan, Effect of martensite volume fraction and its morphology on the tensile properties of ferritic ductile iron with dual matrix structures. J. Mater. Process. Technol. **178**, 44–51 (2006)
3. A. Druschitz, D.C. Fitzgerald. MADI^{TM}: Introducing a New, Machinable, Austempered Ductile Iron, SAE 2003 World Congress & Exhibition. https://doi.org/10.4271/2003-01-0831
4. A. Basso, R. Martinez, J. Sikora, Influence of austenitising and austempering temperatures on microstructure and properties of dual phase. ADI Mater. Sci. Technol. **23**(11), 1321–1326 (2007)
5. M. Erdogan, V. Kilici, B. Demir, Transformation characteristics of ductile iron austempered from intercritical austentizing temperature ranges. J. Mater. Sci. **44**(5), 1394–1403 (2009)
6. V. Kilicli, M. Erdogan, The nature of the tensile fracture in austempered ductile iron with dual matrix microstructure. J. Mater. Eng. Perform. **19**(1), 142–149 (2009)
7. C. Valdés, M. López, M. Figueroa, L. Ramirez, Austempered ductile iron with dual matrix structures. Revista Mexicana De Fisica **55**(1), 48–51 (2009)
8. A. Druschitz, M. Ostrander, R. Aristizabal. The science of intercritically austempered ductile iron (IADI). 71st World Foundry Congress, 19–21, May (2014), Bilbao, Spain
9. J. Aranzabal, G. Serramoglia, D. Rousiere, Development of a new mixed (ferritic-ausferritic) ductile iron for automotive suspension parts. Int. J. Cast Met. Res. **16**(1–3), 185–190 (2003)
10. M. Soliman, A. Nofal, H. Palkowski, Alloy and process design of thermo-mechanically processed multiphase ductile iron. Mater. Des. **87**, 450–465 (2015)
11. J. Shi, S. Zou, R. Smith, J. Too, Effect of elongated graphite on mechanical properties of hot-rolled ductile iron. J. Mater. Eng. Perform. **3**(5), 657–663 (1994)
12. M. Soliman, H. Palkowski, On factors affecting the phase transformation and mechanical properties of cold-rolled transformation-induced-plasticity-aided steel. Metall. Mater. Trans. A **39**, 2513–2527 (2008)
13. M. Soliman, H. Palkowski, Tensile properties and bake hardening response of dual phase steels with varied martensite volume fraction. Mater. Sci. Eng. A **777**, 139044 (2020)
14. H. Bhadeshia, *Bainite in Steel*, 2nd edn. (IOM Commercial Ltd, London, 2001)
15. A. Nofal, L. Jekova, Novel processing techniques and applications of austempered ductile iron (REVIEW). J. Univ. Chem. Technol. Metall. **44**(3), 213–228 (2009)
16. M. Takahashi, H.K.D.H. Bhadeshia, The interpretation of dilatometric data for transformations in steels. J. Mater. Sci. Lett. **8**, 477–478 (1989)
17. ASM Handbook, Vol. 8, Mechanical Testing and Evaluation, ASM Int., (Materials Park, OH, 2000), 146